Spin Dynamics in Single-Molecule Magnets and Molecular Qubits

Daniel Aravena and Eliseo Ruiz*

Departament de Química Inorgànica i Orgànica and Institut de Recerca de Química Teòrica i Computacional, Universitat de Barcelona,

Diagonal 645, 08028 Barcelona, Spain

Departamento de Química de los Materiales, Universidad de Santiago de Chile, Santiago 9170022, Chile

email: eliseo.ruiz@qi.ub.es

Abstract

Over recent decades, much effort has been made to lengthen spin relaxation/decoherence times of single-molecule magnets and molecular qubits by following different chemical design rules as maximizing the total spin value, controlling symmetry, enhancing the ligand field or inhibiting key vibrational modes. Simultaneously, electronic structure calculations have been employed to provide an understanding of the processes involved in the spin dynamics of molecular systems and served to refine or introduce new design rules. This review focuses on contemporary theoretical approaches focused on the calculation of spin relaxation/decoherence times, highlighting their main features and scope. Fundamental aspects of experimental techniques for the determination of key Single Molecule Magnet/Spin Qubit properties are also reviewed.

1. Introduction

The chemical synthesis of paramagnetic molecules featuring increasingly longer magnetic relaxation and spin coherence times, is the main challenge for two intimately linked research areas: Single-Molecule Magnet (SMM)[1-6] and Molecular Spin Qubit research.[7,8] To achieve such objectives, spin dynamics of molecular systems must be tuned to suppress a series of relaxation mechanisms, depending on intra- and inter-molecular interactions. The main molecular factors influencing magnetic relaxation are the energy separation of electronic states, their magnetic anisotropy, molecular vibrations, and dipolar and hyperfine interactions. Environmental molecules can also affect spin relaxation though long-range spin–spin interactions (dipolar electron-electron and hyperfine electron-nuclear) and vibrational coupling. In the case of SMMs, uniaxial magnetic anisotropy must be enhanced, and electronic energy gaps must be as high as possible. Vibrations must be tuned to minimize vibronic coupling, either by symmetry control or by hampering molecular displacements in the magnetically relevant atoms. Detuning vibrational and electronic transition energy has been proposed as a convenient strategy for improving SMMs. On the other hand, molecular spin qubits can be derived from magnetically anisotropic[9,10] or isotropic[11-13] systems. For both SMMs and molecular spin qubits, hyperfine and dipolar interactions must be supressed to prolong demagnetization and coherence times. Providing a mechanistic description of spin dynamics is a necessarily complex task since a comprehensive picture must consider electronic and vibrational aspects of the molecular system and its interaction with surrounding nuclear and electronic spins. In this sense, the study of spin dynamics in molecular systems is a multidisciplinary field involving resonance spectroscopies, molecular magnetism and theoretical chemistry.

2. Experimental Methods

2.1 Spin Relaxation Times determined with Electronic Paramagnetic Resonance

Experimental practice for the determination of spin relaxation times is usually different for qubit molecules and SMMs. In the case of qubit molecules, electronic paramagnetic resonance (EPR) is

usually employed.[14-18] EPR measurements can be performed in single-crystal or powder samples also in frozen solution. The latter is often advantageous since solution samples present a lower concentration of magnetic molecules per unit volume, diminishing the interactions between magnetic centres and, increasing the spin relaxation time. The conventional approach is to use pulsed EPR, allowing the pulses to align the spin in a determined direction and to measure the time required to recover the initial orientation. There are two crucial parameters: the spin–lattice (or longitudinal) T_1 and the spin–spin (or transversal) T_2 relaxation times.[17]

The spin–lattice relaxation process involves the interaction of the spin with the vibrations of the surrounding lattice; consequently, T_1 depends on the temperature. The energy exchange between the vibrations and the spin provides the mechanism that produces the spin relaxation. There are several methods that use the EPR technique, determining T_1 time as the timescale for the evolution of magnetization along the z axis.[18] Taking the initial magnetization M_0, and subsequent spins in the $+z$ direction aligned by an external magnetic field, the T_1 time can be determined by applying a π microwave pulse inducing a 180º rotation of the magnetization. Analysis of the evolution time of the M_z component until the system recovers the initial direction allows us to extract the T_1 value using the Bloch equation:

$$M_z = M_0(1 - e^{-t/T_1}) \qquad (1)$$

In many cases, a multi-pulse experiment is performed because the system does not follow the simple exponential Bloch equation due to the presence of other spin processes. These processes are usually called spectral diffusion, which encompasses several different contributions including motion of an anisotropic paramagnetic centre, electron-electron exchange, electron-nuclear cross relaxation and nuclear spin flip-flops.[18] A general strategy for avoiding the presence of spectral diffusion effects is to increase the length of the saturating pulse until a constant relaxation time is reached, thus T_1 is directly determined without any other superposed effects. In some cases, it is

possible to improve the fitting with a simple modification of Equation 1 by introducing the effect of additional contributions through the β stretching parameter:

$$M_z = M_0(1 - e^{-(t/T_1)^{\beta}}) \qquad (2)$$

If this does not improve the fitting, it is necessary to add in the mathematical expressions corresponding to the spectral diffusion contributions. In a multi-pulse experiment to determine T_1, one initial π pulse is performed and after a delay of time T, a spin-echo sequence (π/2–τ–π–τ Hahn-echo[19] see Figure 1) is used (echo-detected inversion recovery approach). A similar method can also be employed if the initial pulse is a long low-power pulse. This is called echo-detected saturation recovery method. Analysis of the recovering curve of the echo amplitude until equilibrium is reached, as a function of the time T, allows us to estimate the T_1 value.

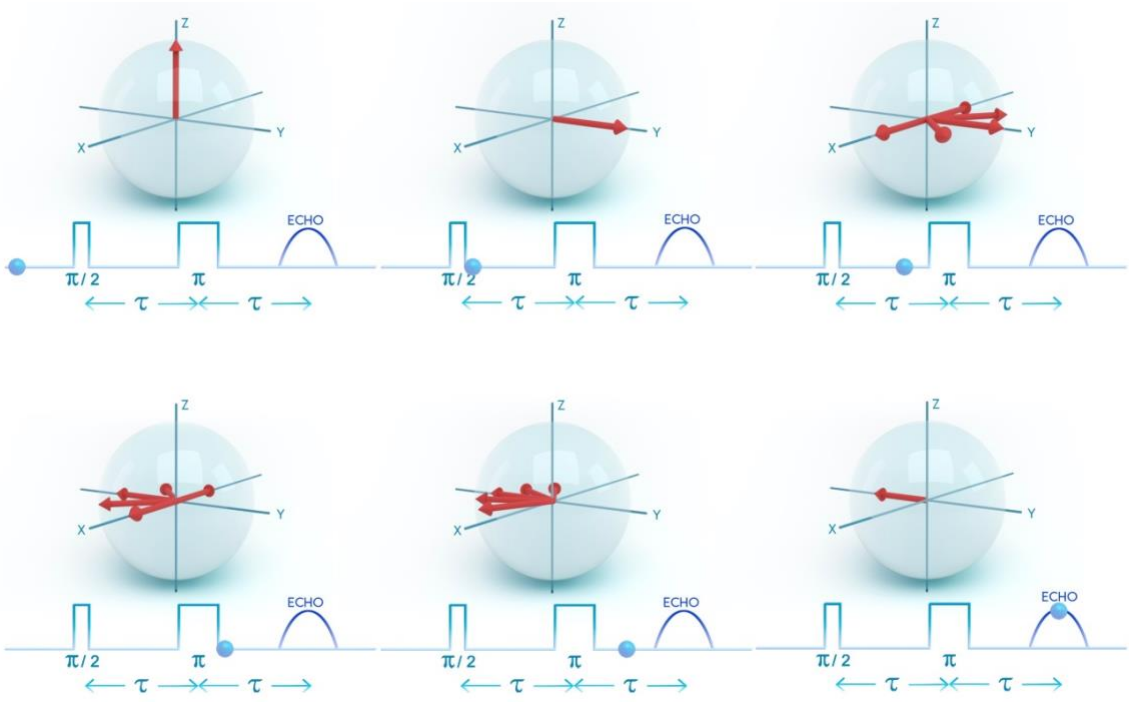

Figure 1. π/2–τ–π–τ Hahn echo employed to determine the spin relaxation times.

The spin–spin relaxation involves the T_2 time that follows the temporal evolution of magnetization in the *xy* plane until recovery of thermal equilibrium. Usually, T_2 is considerably smaller than T_1, thus the spin reorientation in the *xy* plane is much faster than in the *z* axis. However, as T_1 decreases

with increasing temperature, in some cases at higher temperatures both magnitudes could be similar. There are also several methods to determine T_2. Again, the simplest method would be to apply a $\pi/2$ pulse and follow the evolution of the M_x component according to the following equation:

$$M_x = M_0 e^{-t/T_2} \quad (3)$$

Multi-pulse approaches are also employed for the *xy* spin relaxation, using the $\pi/2-\tau-\pi-\tau$ Hahn echo, modifying the τ time between the pulses to overcome the problems of fitting with a simple model (Eq. 3).[18] The spin echo dephasing time constant, usually known as phase memory decay time T_m, can be determined from the representation of the echo amplitude as a function of τ time.[20] The longer the delay of τ time after the $\pi/2$ pulse, the larger the number of dephased spins; a lesser number will be refocused with the π pulse, resulting in a decrease of the *xy* magnetization. An exponential decay of the echo signal with the τ time is expected, and such decay is proportional to $\exp(-2\tau/T_m)$. Thus, a fitting procedure allows us to determine the T_m magnitude, including all the processes that produce loss of electron spin phase coherence, T_2 being one of them. If the system follows the Bloch equation (Eq. 3), we can assume that $T_m=T_2$ because other contributions such as librational motion of the paramagnetic species (sometimes important at high temperatures) and nuclear spin diffusion are negligible. Sometimes, in the fitting procedure to extract T_m, it is mandatory to introduce a stretching factor, as in Eq. 2, or to employ a biexponential function with two different phase memory times, $T_{m,f}$ and $T_{m,s}$ (fast and slow, respectively), indicating two dephasing mechanisms with different timescales. Analysis of the dependence of T_m on the temperature (T_2 is temperature independent) can provide some insights into the additional contributions.

Other useful EPR measurements for molecular qubits include variable power nutation experiments to show the coherent spin behaviour. In such experiments, the thermal equilibrium along the $+z$ direction is reached by the alignment of the magnetization with an external field B_1.[18] Then,

microwave pulses of a certain duration t_p and B_1 value are applied. Thus, a rotation of the spins is performed by an increasing nutation angle that depends on t_p and B_1. The representation of the *z*-component of the magnetization with the t_p values shows the typical oscillatory pattern of the Rabi oscillations (Rabi nutation frequency $\omega_1=\mu_B \cdot g \cdot B_1/\hbar$) proving that the qubit can be placed in an arbitrary state superposition in the Bloch sphere. It is important to keep in mind that the oscillations can be damped by the spin relaxation, when such processes can be observed only in slow spin–spin relaxation, $1/T_2 << \omega_1$.

2.2 Spin Relaxation Times determined with AC Susceptibility

Analysis of the spin relaxation time for single-molecule magnets is usually performed by measuring alternating current (ac) magnetic susceptibility with, for instance, a SQUID device. Data on ac susceptibility can be analysed within the extended Debye model, in which a maximum in the out-of-phase component χ_M'' of the complex susceptibility is observed when the spin relaxation time τ equals $(2\pi\nu)^{-1}$.[3] The Cole-Cole expression is introduced to describe distorted Argand plots,

$$c_{ac}(w) = c_S + \frac{(c_T - c_S)}{1 + (iwt)^{1-a}} \qquad (4)$$

where $\omega = 2\pi\nu$, and χ_T and χ_S are the isothermal and adiabatic susceptibilities *i.e.*, the susceptibilities observed in the two limiting cases $\nu \rightarrow 0$ and ∞, respectively. The α parameter (between 0 and 1) describes the distribution of relaxation times; the wider the distribution, the larger is α. If α is equal to 0 there is only one single τ value. The frequency dependence of χ_M' and χ_M'' can be split into:

$$\chi_M'(\omega) = \chi_S + \frac{(\chi_T - \chi_S)[1+(\omega\tau)^{1-\alpha}\sin(\pi\alpha/2)]}{1 + 2(\omega\tau)^{1-\alpha}\sin(\pi\alpha/2) + (\omega\tau)^{2-2\alpha}}$$

$$\chi_M''(\omega) = \frac{(\chi_T - \chi_S)[(\omega\tau)^{1-\alpha}\cos(\pi\alpha/2)]}{1 + 2(\omega\tau)^{1-\alpha}\sin(\pi\alpha/2) + (\omega\tau)^{2-2\alpha}} \quad (5)$$

From this kind of measurement it is possible to fit the τ values, temperature and external magnetic field[21] that can be modified in the experiment. It is worth noting the papers of Ho and Chibotaru which provide an analysis of the results for systems showing two maxima in the ac susceptibility that can appear even in mononuclear systems.[22,23]

2.3 Comparison Spin Relaxation Times using different Techniques

In principle, τ can be identified with the spin–lattice T_1 relaxation time determined by EPR. The comparison between these magnitudes is not straightforward because in most cases the EPR samples are diluted to avoid decoherence. Such a process is induced by spin–spin interactions, either electron-electron or electron-nuclear. Hence, dilution in diamagnetic matrices or solution using solvents with elements with or without reduced nuclear spin, for instance CS_2 or deuterated solvents, help to increase T_2 values determined by EPR.[24] The use of solutions complicates the comparison with ac-susceptibility relaxation times because such measurements are usually taken in powder, and the molecular environments are completely different. Dilution in diamagnetic matrices is also a problem for susceptibility measurements due to the low percentage of magnetic species in the sample. Thus, it is difficult to compare the spin–lattice relaxation times determined by EPR and susceptibility measurements. Among the few reported examples with both sets of data available, it is worth mentioning the studies of Sessoli et al., which focused on vanadyl phthalocyanine complex.[25-31] This molecule shows room temperature coherence time of around 1 μs at 300 K despite the presence of hydrogen atoms diluted in the diamagnetic titanium analogue. At room temperature, T_1 and T_m have similar values.[26] For this system, the τ value extracted from susceptibility measurements is around 0.04 ms (at 5 K and external field of 0.08 T) for either the

bulk or 1:10 diluted samples.[26] The EPR value at low temperature for the same diluted sample is not available, but for a 1:1000 dilution, that should have a strong influence on T_2 and not on T_1, the T_1 value is 14 ms (at 4.3 K). The same VOPc molecule in a 0.5 mM solution of D_2SO_4/H_2SO_4 has T_1 values of 226 ms and 2405 ms, at 7 K, with a double exponential fitting by van Slageren and others.[32] Also, Sessoli et al. studied the $[Ph_4P]_2[VO(dmit)_2]$ and $[Ph_4P]_2[V(dmit)_2]$ complexes.[11] The susceptibility τ values for the bulk samples are 0.12 ms (at 5 K and external field 0.02 T) and 0.025 ms (at 5 K and external field 0.1 T), respectively. The EPR T_1 values of the diluted samples in diamagnetic matrices are 24 ms and 10 ms at 4.3 K, respectively. The dilution clearly affects the time relaxation values, as we can see in next section, not only are spin–spin contributions modified in the diluted samples, but also some spin relaxation mechanisms, such as quantum tunnelling.

2.4 Complexes with Long Coherence Times

For the practical application of the qubits, it is vital to reach a reasonable coherence time, usually quantified with a figure of merit as the $\omega_1 \cdot T_m$ product, Rabi nutation frequency by phase memory decay time, of around 10^4-10^5.[7,33,34] The usual ω_1 values are around 10^7 s^{-1} (10 MHz), thus T_m (or in general T_2) must be larger than 10^{-4} s (0.1 ms). A detailed discussion of the best molecular qubits according to their coherence time can be find in recent review papers,[7,8,12,24,34] but the usual T_m times in an environment similar to a device are smaller than such a threshold. A record value was obtained with a deuterated vanadium complex $[Ph_4P]_2[V(C_8S_8)_3]$ using a nuclear spin-free dithiolene $C_8S_8^{2-}$ ligand, by Zadrozny, Freedman et al.,[12] in a solution of a similarly nuclear spin-free solvent CS_2, to give a T_m value of 0.7 ms at 10 K. However, despite this case, which utilized the most favourable conditions, the typical T_m values for diluted mononuclear transition complexes, usually with low spin ions such as V^{IV} or Cu^{II},[12,30,31,35-41]are still in the approximate range of 0.01-0.001 ms. [7,24] A systematic study of the coherence time of heteronuclear Cr_7Ni wheel systems was carried out by Winpenny et al.,[13,42-48] showing T_2 values in the range of 0.0003-0.015

ms. Similar coherence times have been obtained with lanthanide systems. Coronado et al. have proposed molecular qubits by using polyoxometalate systems to provide a protective nuclear free spin to the lanthanide due to the low abundance of the non-zero nuclear spin isotopes of Mo and W elements. [8,9,49-55] As high spin and large magnetic anisotropy systems are unsuitable for qubits, the studies have mainly focused on systems with relatively small magnetic anisotropy, such as Gd^{III} compounds or Ho^{III} with a $4f^{10}$ configuration. Also, Pedersen et al. performed extensive studies of a molecular spin qubit based on Yb^{III} cations coordinated to a Schiff-base ligand (trensal).[10,56] A diluted sample in the Lu^{III} analogue presents a T_2 value of 0.005 ms. The potential application of these molecular systems as qubits is mainly to use them in superconducting microwave resonator devices.[27,57,58] However, coherence times for the molecular systems are still relatively far off those regularly obtained by doping diamond and silicon with N or P atoms with T_2 values reaching 1-5 ms at room temperature.[59-61]

3. Spin Relaxation Mechanisms

3.1 Spin Relaxation Mechanism through Phonons

Due to the multitude of interactions associated with spin relaxation, several magnetic relaxation mechanisms are described in the literature. First, we focus on mechanisms involving energy exchange with the environment through phonons.

Direct Process. Under the influence of an external magnetic field B, the splitting of the states due to the Zeeman effect results in a spin flip energy that is an exact match with one lattice phonon energy.[17] For Kramers systems with half-integer spin values, an admixture with electronic excited states is required, as pointed out by van Vleck, to break the time-reversal symmetry principle.[62] The hyperfine coupling producing an admixture of states can be effective in breaking such a principle.[63] For the direct spin relaxation mechanism for a Kramers system, the rate can be expressed by the following equation:

$$T_1^{-1} = A\, B^4\, T \qquad (6)$$

where *A* is an adjustable parameter, *B* is the external magnetic field and *T* is the temperature, while an equivalent term with the relaxation rate proportional to B^2 is used for non-Kramers species.[64]

Raman Process. This is a mechanism involving a two-phonon process with a virtual excited state with an energy smaller than the Debye temperature.[65] The relaxation rate can be expressed as,

$$T_1^{-1} = C\, T^n \qquad (7)$$

where *C* is a constant parameter, *T* the temperature and *n* is 7 and 9 for non-Kramers and Kramers systems, respectively. In practice, *n* is treated as an adjustable parameter and can strongly deviate from its theoretical temperature dependence. The energy in the transfer from the spin system to the lattice is the difference between absorption and emission to the virtual state (see Fig. 2). In some cases, there are few available phonons with the appropriate energies for exchange with the spin. Thus, there is a less efficient relaxation mechanism, and a similar equation (Eq. 7) is proposed with *n*=2 (phonon bottleneck).[66] van Vleck introduced a dependence with the external field of the constant parameter C,[62] resulting in

$$T_1^{-1} = d\left(\frac{1+e\cdot B^2}{1+f\cdot B^2}\right) T^n \qquad (8)$$

In the field-dependent Raman term, usually known as Brons-van Vleck equation, the *d* parameter corresponds to the zero-field relaxation, the *e* parameter is highly dependent on the paramagnetic centre's concentration and introduces the relaxation of the interacting spins and finally, the *f* parameter reports the effect of the external field on suppressing the spin relaxation. Eq. 8 was proposed by van Vleck for S=1/2 Cu^{II} and S=3/2 Cr^{III} compounds.[62] However, recently the field-dependent Raman term was mainly used only to fit the experimental data of S=1/2 systems, mostly V^{IV} complexes.[11,26,30] In these studies, instead of Eq. 8, the mathematical expression of the Raman relaxation was split in two terms. The first one is only temperature dependent (Eq. 7) while the field-dependent term is the prefactor of T^n in Eq. 8 that depends of the *d*, *e* and *f* parameters. This field dependence Raman term has a similar mathematical expression than the quantum tunnelling

relaxation (see section 3.2, Eq. 12), this fact should be carefully considered in the fitting procedures.

Recently, Ho and Chibotaru have developed a theoretical model to handle Raman contributions together with the direct mechanism.[67] Their results indicate that for rigid Kramers systems, the Raman mechanism is independent of the magnitude of the external field but dependent on its orientation. Furthermore, the Raman process in non-Kramers systems is mostly suppressed by the application of an external magnetic field that breaks the resonance. They also proposed that the temperature dependence of the Raman term for both Kramers and non-Kramers systems is T^9, despite traditionally being considered as T^7 for non-Kramers systems. Chiesa et. al performed a detailed study on the magnetization dynamics of a dysprosocenium SMM with high blocking temperature.[68] Combining ac- magnetometry and nuclear magnetic resonance measurements, field and temperature dependent relaxation times were determined. Furthermore, the phonon density of states was obtained inelastic neutron scattering experiments. This information was complemented with ab initio calculations to disentangle the different mechanisms contributing to demagnetization. Authors highlight the importance of acoustic phonons for the Raman regime.

Orbach Process. Like the Raman mechanism, this is also a two-phonon process, but the intermediate state involves an electronic excited state of the system:[17] The temperature dependence of the Orbach mechanism is exponential.

$$T_1^{-1} = A\ \frac{E^3}{e^{E/k_BT}-1} \approx A\ E^3\ e^{-E/k_BT} \qquad (9)$$

Where *A* is a constant parameter, E the energy of the excited state and T the temperature. The approximation is valid for E >> k_BT. Thus, from the fitting of T_1^{-1} at different temperatures, it is possible to extract the energy barrier involved in this process, corresponding to the excited state allowing for spin relaxation. The spin inversion process can be due to a complete jump of the energy barrier through the highest low-spin excited state of the multiplet or helped by an efficient

quantum tunnelling relaxation in one of the intermediate excited states. It is worth mentioning that in S=1/2 systems with only two degenerate states, the Orbach process is ill-defined.

Local-mode Process. This is a similar mechanism to the two-phonon processes previously described, but here, the involved state is a vibrational excited state of the electronic ground state.[69] The mathematical expression is similar to that for the Orbach process, but the energy involved corresponds to a vibrational energy $\hbar\omega$ of the system:

$$T_1^{-1} = C_{loc}\left(\frac{e^{-\hbar\omega/k_B T}}{(e^{-\hbar\omega/k_B T}-1)^2}\right) \quad (10)$$

Despite recent studies that have analysed the importance of the spin–phonon coupling in the relaxation processes, this local term is not usually included in the analysis of the T_1^{-1}dependence on temperature. An expression similar to Eq. 10 can be employed to simulate the effect of thermally activated processes such as the rotation of some groups of the molecules [20] when the involved E_{th} energy is comparable to the Larmor (precessional) frequency ω_L of the magnetic moment,

$$T_1^{-1} = C_{th}\left(\frac{e^{\frac{E_{th}}{k_B T}}}{1+\omega_L{}^2 e^{-\frac{2E_{th}}{k_B T}}}\right) \quad (11)$$

C_{th} being a constant. The main difference between this relaxation contribution and Raman, local-mode and Orbach is the dependence of the Larmor frequency. See Fig. 2 for a pictorial description of the spin relaxation mechanisms through spin–lattice processes.

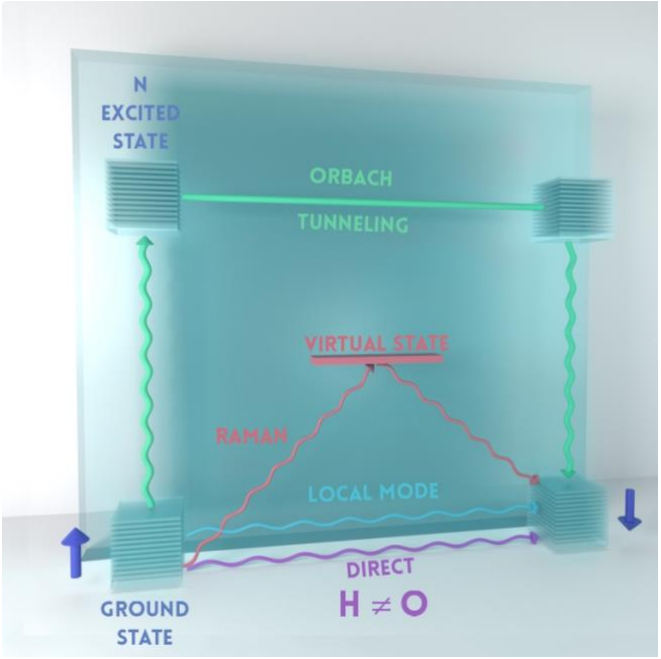

Fig. 2 Scheme of the spin relaxation mechanisms based on spin–lattice processes from an electronic ground state (and vibrational states).

3.2 Spin-Spin Relaxation Mechanisms and Quantum Tunnelling

The second main group of spin relaxation mechanisms are those involving the spin–spin interactions, which consider both hyperfine (electron-nuclear spin) and dipolar (electron-electron) terms.[70,71] Some of these interactions will be intramolecular (i.e. by the presence of $I \neq 0$ nuclei or more than one paramagnetic centre in the same molecule) or intermolecular (by magnetic centres belonging to neighbour molecules). Strategies to supress these interactions include magnetic dilution (replacement of a fraction of crystallized magnetic molecules by diamagnetic analogs)[72], replacement of atoms with I=0 isotopes[73,74] or the preparation of frozen solution samples with nuclear spin-free solvents.[12] The latter approach will supress both hyperfine and spin dipolar relaxation. The spin-spin relaxation time (T_2) is employed to quantify these relaxation processes. This parameter is of prime importance for the coherence time, which is the key parameter in the design of molecular spin qubits.[26]

For an isolated Kramers doublet system, quantum tunnelling is forbidden by the time-reversal symmetry principle.[62] However, the presence of spin–spin interactions causes a dipolar broadening of the energy levels, allowing spin relaxation though quantum tunnelling.[75] Prokof'ev and Stamp[76] explained the low temperature tunneling relaxation for Mn_{12} and Fe_8 considering the dynamic nature of hyperfine and dipolar interactions. For short times, tunneling relaxation was predicted to have a $\sqrt{t}$ dependence due to the effect of rapidly oscillating hyperfine bias field, which induces spin flips, modulating the dipolar field and allowing for further spin relaxation. At long times, the time dependence is better represented by an exponential function. Under this model, the tunneling rate depends on the nuclear T_2, the tunneling gap matrix element between the tunneling doublet and the spatial distribution of internal fields. This phenomenology was experimentally corroborated by Wernsdorfer et al. for the Fe_8 SMM,[77] providing a practical setup for the estimation of relevant tunneling parameters.

A external magnetic field induces an energy gap in the tunnelling doublet, supressing relaxation. Field dependence of tunnelling relaxation time is usually adjusted to the following expression:

$$T_1^{-1} = \frac{1+B_1}{1+B_2 \cdot B^2} \qquad (12)$$

where B_1 and B_2 are constant parameters. Spin relaxation by tunnelling is not only associated with the ground state, but excited states can also exhibit relaxation associated to this mechanism, in a process called thermally assisted quantum tunnelling.[78] Recently, Ding et al. analysed the field and temperature dependence for the relaxation dynamics of $[Dy(tBuO)Cl(THF)_5][BPh_4]\cdot 2THF$.[79] In the low temperature region, authors found noticeable temperature dependence of the relaxation time and proposed the following expression to account for tunnelling:

$$T_1^{-1} = \frac{(2\omega)^i \eta^{i-1}}{1+\left(\eta g_{eff} \mu_B \hbar^{-1} B\right)^i} \qquad (13)$$

where η^{-1}corresponds to the characteristic phonon collision rate of the lattice that shows an exponential temperature dependence, ω is a perturbation that quantifies the mixing between $\pm m_J$ ground-state wave functions, $\hbar\omega$ is the tunnelling gap and i is the field exponent. A small

tunnelling gap (around 10^{-3}-10^{-5} cm^{-1}) indicates an efficient tunnelling relaxation, thus, the experimental fitting of such parameters allows to determine its magnitude. Furthermore, large tunnelling gap values (1 cm^{-1} ≈30 GHz) might be suitable to be determined by pulsed EPR and it is a key ingredient for long coherence times and insensitivity to magnetic noise in molecular qubits.[51]

3.3 Determination of Parameters of the Spin Relaxation Mechanisms

The spin relaxation mechanisms provide the mathematical framework to fit the experimental spin relaxation times obtained using EPR or ac-susceptibility measurements. Usually, susceptibility measurements of powder samples can be used, according to Eq. 5, to determine the relaxation τ values. Due to the large number of fitting parameters, the largest possible amount of experimental data is recommended for a proper fit. For a S >1/2 system, the expression to fit the temperature and external field dependence of τ can include direct, Raman, Orbach, local-mode and tunnelling terms,

$$\tau^{-1} = A\,B^4\,T + C\,T^n + D\,e^{-E/k_BT} + C_{loc}\left(\frac{e^{-\hbar\omega/k_BT}}{(e^{-\hbar\omega/k_BT}-1)^2}\right)+\frac{1+B_1}{1+B_2\cdot B^2} \qquad (14)$$

while for S = ½, the Orbach term is not considered,

$$\tau^{-1} = A\,B^4T + d\left(\frac{1+e\cdot B^2}{1+f\cdot B^2}\right)T^n + C_{loc}\left(\frac{e^{-\hbar\omega/k_BT}}{(e^{-\hbar\omega/k_BT}-1)^2}\right)+\frac{1+B_1}{1+B_2\cdot B^2} \qquad (15)$$

As mentioned above (see section 3.1) Brons-van Vleck field dependence of the Raman contribution is mostly employed in S=1/2 systems despite that it was originally included to study S=1/2 and S=3/2 compounds.[62] Thus, the second term of Eq. 14 could be replaced by the equivalent field-dependent contribution of Eq. 15. In most reported studies of SMM systems, only the Orbach term is considered to extract the energy barrier that corresponds to the energy of the excited state involved in the spin relaxation process.[1-3,5] Thus, with just the slope of the representation of log(τ) vs 1/T in the linear dependence region it is possible to determine the energy barrier. Nevertheless, despite over parametrization problems, the determination of the parameters has often

been performed. However, as mentioned above, the local-mode term is not usually included in the fitting of the data. It is worth noting the analysis of susceptibility data performed by Zheng and others.[79] They studied a family of mononuclear Dy^{III} complexes for the dependence of the relaxation rate on temperature and the external field, using ac and dc measurements. The field-dependent data was extracted from the time evolution of dc magnetization using a stretched exponential decay model. The analysis of a large amount of relaxation rate data allowed for an accurate determination of the main relaxation mechanisms for the different temperatures and external fields.

4. Theoretical Approaches for Spin Relaxation

Spin dynamics have been extensively studied by means of classical approaches such as the Landau-Lifshitz-Bloch equation of motion.[80] This methodology is phenomenological and allows to estimate the time evolution of magnetization in terms of the gyromagnetic ratio and a damping parameter. However, quantum effects are not considered in this method and it cannot be directly applied to the spin relaxation of single-molecule magnets and molecular qubits. Some attempts to include such effects have been carried out for single-molecule magnets.[81]

4.1 Direct Calculation of the Spin Relaxation Times (T_2 and T_m)

The direct calculation of the spin relaxation times T_1 and T_2 from electronic structure methods is not a trivial task, due to the importance of different parameters as lattice vibrations, magnetic anisotropy, temperature, electron spin–spin interactions, spin nuclear effects and so on. Hence, there is an increasing number of theoretical proposals focusing on different aspects of spin relaxation/dephasing, where a comprehensive model is still an open challenge in this field.

A simple procedure for obtaining a rough estimation of T_2 is to consider the expression proposed by Bloembergen et al.,[70] in which the spin dipolar interactions are proportional to r^{-3}, with r being the distance between the spins (electron-nuclear terms could also be considered). Escalera-Moreno

et al. proposed a method to calculate the phase memory time T_m for samples with a high concentration of electronic spins,[82] based on a previous model by Stamp and others.[83] This model focuses on systems presenting instantaneous diffusion as the limiting decoherence mechanism and is particularly suited for describing T_m at zero first-order Zeeman shift conditions (ZEFOZ or clock transitions). As the Zeeman effect progressively vanishes up to first order at clock transitions, the molecular qubit becomes insensitive to magnetic interactions related to neighbour nuclear and electronic spins. Thus, decoherence mechanisms associated with these interactions are largely supressed, and relatively long T_m values can be reached even for non-diluted samples with large spin–spin interactions. The T_m values arising from the nuclear and electron-spin baths are calculated using the following expression:

$$T_m^{n+e} = \frac{\hbar\Delta}{\mathrm{E}_n^2+\mathrm{E}_e^2} \qquad (16)$$

where Δ is the energy gap between the two given magnetic states and E_n^2 (E_e^2) is the nuclear (electron) contribution to the echo line half-width. A reasonable reproduction of the experimental T_m values for a Ho^{III} polyoxometalate and a copper(II) phthalocyanine complex[82] was obtained. In a subsequent paper this model was applied to a Gd^{III} polyoxometalate qubit candidate.[84]

Recently, Chen et al.[85] performed a theoretical study of spin relaxation in a family of mononuclear vanadyl complexes synthesized by Freedman and others.[86,87] These four complexes $(Ph_4P)[VO(C_{n+1}H_6S_n]_2)$ (n= 2,4,6, and 8) show an increase of the distance between the paramagnetic vanadyl centre and the hydrogen nuclei that has non-zero nuclear spin. Authors focused on the hyperfine electron-nuclear interaction by calculating the hyperfine coupling constants using DFT methods. These parameters were later employed to solve the time-dependent Schrödinger equation. The electron spin decoherence time is estimated through a cluster-correlation expansion scheme[88] that allows to calculate the Hahn echo decay for the four metal complexes. The long-time plateau of the calculated echo decay curve (residual coherence) as proposed as a convenient molecular descriptor for T_2. This parameter is molecular since it depends

on the interaction of the electronic spin with nuclear spins from the same molecule. The effect of counterion nuclear spins was also considered, showing an important role of spin dephasing.

4.2 *Ab Initio* Calculations for Magnetic Anisotropy and Spin–Lattice Relaxation

As mentioned above, strong uniaxial magnetic anisotropy is absolutely necessary to obtain high performance SMMs, while this requirement is not so strict for molecular spin qubits. Accordingly, theoretical methods describing SMMs must be particularly accurate when describing magnetic anisotropy. The direct use of time-dependent Density Functional Theory (TD-DFT) to calculate the low energy state manifold responsible for magnetic relaxation is problematic since DFT is a monodeterminant methodology, and incapable of properly describing wave functions associated with systems with large magnetic anisotropy. Multiconfigurational methods, mainly those based on the complete active space self-consistent field (CASSCF), including scalar relativistic and spin–orbit effects can provide an accurate description of the magnetic anisotropy for mononuclear complexes. In order to corroborate the descriptions provided by these theoretical methods, it is possible to perform a comparison of the g-components, magnetization, and magnetic susceptibility with experimental data. For polynuclear systems, the substitution of all the paramagnetic cations, but one, with diamagnetic ones, allows us to determine the local magnetic anisotropy of each paramagnetic centre in an independent calculation. The calculation of the exchange interactions between highly anisotropic magnetic centres of polynuclear systems remains an open challenge, despite some recent advances.[89] van Slageren et al. have reported a CASPT2 approach applied to more than one group of open-shell orbitals[89] focusing in a dinuclear Yb^{III} complex previously reported by Winpenny and collaborators.[90,91] Up to now, the most common option has been to extract exchange interaction parameters[92] by fitting experimental magnetization and susceptibility data using the calculated local anisotropy of each magnetic centre.[93]

***Ab Initio* Calculations for Magnetic Anisotropy.** The main success of electronic structure methods in analysing spin relaxation in single-molecule magnets was in providing a qualitative

description of the relative importance of the spin relaxation mechanism and some information about the states of the molecule involved in Orbach and quantum tunnelling processes. Chibotaru et al.[94-98] employed multiconfigurational *ab initio* calculations to estimate transition matrix elements for the magnetic dipole operator over relativistic states. These matrix elements are considered to be proportional to the transition rates between pairs of states and can be employed to derive relaxation pathways by identifying the largest matrix elements connecting both sides of the double well potential. One example of such studies is represented in Fig. 3.

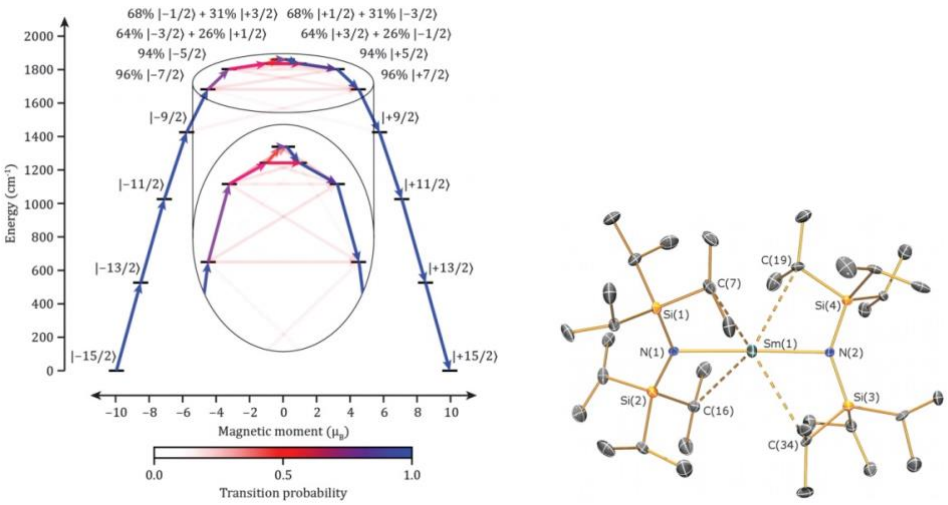

Figure 3. Electronic states and magnetic transition probabilities for a hypothetical linear Dy^{III} complex, see analogous Sm^{III} system, calculated at CASSCF level.[99]

One of the main steps towards increasing the magnetic anisotropy of lanthanide complexes is to reach a linear coordination[99,100] that will result in an Orbach/tunnelling relaxation mechanism through a high-excited state (see Fig. 3). The sixth excited Kramers doublet has an efficient tunnelling effect for the hypothetical $[(Pr_3Si)_2N–Dy–N(SiPr_3)_2]^+$, proposed by Chilton et al.,[99] resulting in an energy barrier close to 2000 cm^{-1}. The lack of stability of two-coordinate linear Dy^{III} complexes has promoted the use of ligands with higher coordination while keeping a similar coordination structure, such as the dysprosocenium complexes that are single-molecule magnets presenting record blocking barriers up to 80 K.[101-103] For the 80 K record molecule [(η^5-Cp*****)Dy(η^5-Cp^{iPr5})][$B(C_6F_5)_4$], CASPT2 calculations predict the spin relaxation through the fourth

excited Kramer doublet (at 1524 cm-1), very close to the experimental fitted U_{eff} demagnetization barrier of 1542 cm-1. The relation between demagnetization barrier and blocking temperature is not direct since complexes with similar barriers can have contrasting blocking temperatures. For instance, the pentagonal bipyramidal $[Dy(^{t}BuO)_2(pyridine)_5][BPh_4]$ complex (see Fig. 4) has a very high U_{eff} = 1815 K (1261 cm-1), but the blocking temperature is only 3 K.[104]

One of us proposed a theoretical approach to calculate the relaxation time due to the tunnelling effect between any Kramers doublet, ground or excited. From this information, the effective demagnetization barriers can be calculated.[75] The intermolecular spin–spin dipolar interaction produces a broadening of the single-molecule levels, allowing the quantum tunnelling. It is possible to determine the tunnelling relaxation rate for each Kramers doublet $k_{QT,i}$. Assuming an Orbach regime with a fast-thermal excitation and slower excited-state tunnelling, the demagnetization rate for each Kramers doublet is expressed as,

$$k_i\ (T) = \frac{\exp\left(^{-E_i}/_{KT}\right)}{Z} k_{QT,i} \qquad (17)$$

where E_i is the excitation energy of the *i* doublet determined at CASSCF level, and *Z* is the partition function. We can define the effective demagnetization barrier as,

$$U_{eff}(T) = \sum_{i=1}^{M} \frac{k_{,i}}{N_k} E_i \qquad (18)$$

where *M* is the number of Kramers doublets involved in the spin relaxation and N_k is a normalization factor for the tunnelling rate. In Fig. 4 we can identify which Kramers doublets are related to large contributions to U_{eff}.[75] In this way, the relaxation pathway is unambiguously calculated. In Fig. 4, spin relaxation mostly starts with the third excited state, with the fifth and sixth excited states being those that contribute towards reaching a calculated U_{eff} value of 1196 cm-1, close to the experimental value of 1261 cm-1. This model was extended to consider relaxation time enhancement due to magnetic dilution,[105] showing that typical dilution ratios of 10% and 1%

can lead to an enhancement of the tunnelling relaxation time of 2 and 4 orders of magnitude, respectively.

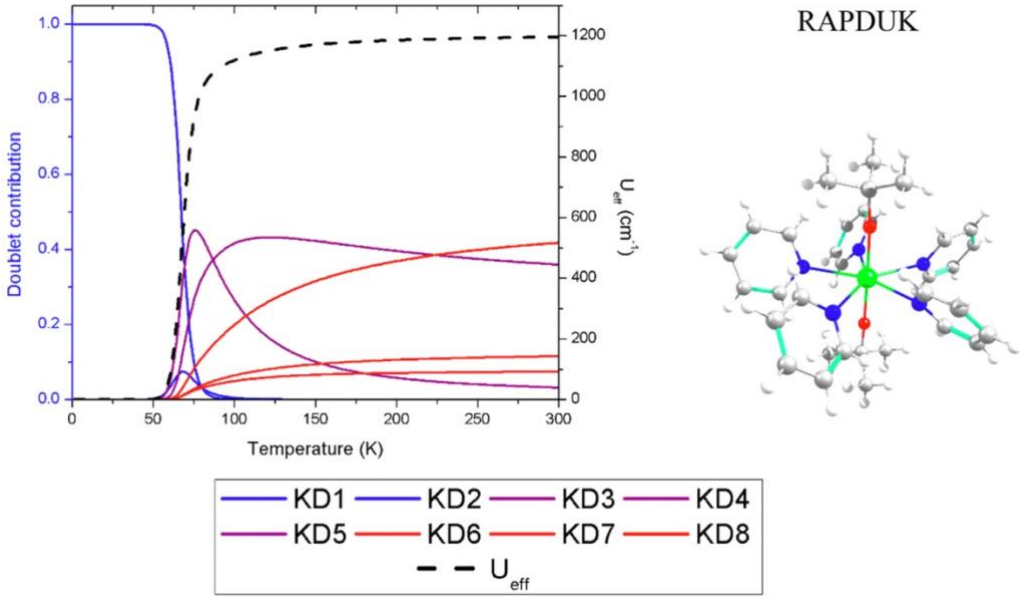

Fig. 4 Calculated contribution of each Kramers doublet and Ueff as a function of temperature for the pentagonal bipyramidal [Dy(tBuO)2(pyridine)5][BPh4] complex (CSD refcode RAPUDUK).[75]

This approach has been recently employed to analyse SMM blocking temperatures.[106] As indicated previously, there is not a clear relationship between both magnitudes with systems with high energy barriers but low blocking temperatures.[104] Castro-Alvarez et al. determined which relaxation mechanism is limiting the blocking temperature for a set of seventeen Dy^{III} complexes with high energy barrier. The best SMMs (T_B > 50K) were mainly limited by Orbach regime, while molecular magnets with lower blocking temperatures showed more important contributions from Raman and tunnelling relaxation. The Orbach limiting temperature corresponds to:

$$T_{Or} = \frac{U_{eff}}{ln\left(\frac{\tau_0}{\tau_{ref}}\right)} \qquad (19)$$

Where U_{eff} as calculated from Eq. 18, τ_{ref} was equal to 100 s, following the usual convention[107] and τ_0 is the Orbach prefactor. For the studied systems, τ_0 as always in a narrow range between 10^{-11}-10^{-12} s, so the denominator in Eq. 19 was always close to 28. This value can be considered

as a convenient approximation for the relation between the effective demagnetization barrier and the Orbach limiting temperature.

Spin-Phonon Coupling Constants. To progress from the calculation of demagnetization barriers to directly estimating the relaxation time at a given temperature, the effect of vibrations must be considered. In recent years, different groups have developed proposals in this direction.[79,108-112] The common strategy is to determine the vibrational modes and corresponding energies with DFT calculations, using periodic or discrete models for the molecules. Once the vibrational modes are determined, the second step is to calculate the spin–phonon coupling for each vibrational mode using a multiconfiguration method such as CASSCF, CASPT2 or NEVPT2. Thus, it is possible to determine which are the most relevant vibrational modes affecting spin relaxation. Normally, this information is fed into a master matrix which eigenvalues are the characteristic rates of the system.

To increase the relaxation time, new molecules must reduce the spin–phonon coupling constants of their vibrational modes. Thus, knowledge of the vibrational modes with larger spin–phonon coupling is crucial to provide a rational design of improved systems. General strategies are: (i) tuning lowest-lying vibrational modes to higher energies to avoid the occupation of such vibrational states at low temperatures, and/or (ii) reducing the vibrational displacements for the paramagnetic ion and its immediate coordination environment.

Sanvito et al. developed a first principles model to study the spin dynamics of mononuclear S=2 Fe^{II} SMMs[113,114] and molecular V^{IV} qubits.[108,115,116] For the [(tpaPh)Fe] complex (tpaPh is the deprotonated form of tris((5-phenyl-1H-pyrrol-2-yl)methyl)amine), authors combined the calculation of phonons at Γ point, using DFT and CASSCF calculations to determine the zero-field splitting parameters and spin–phonon couplings.[114] These parameters are introduced in a spin–phonon dynamics simulation using a master equation to reproduce the temperature

dependence of the τ spin relaxation time and to compare the results with those obtained from the ac susceptibility measurements. In the same study, they also analysed the role of anharmonicity for spin dynamics. More recently, they examined the role of acoustic phonons, showing it to be negligible in diluted samples.[113] The same theoretical approach was employed to study a family of four mononuclear V^{IV} complexes ($[VO(cat)_2]^{2-}$, $[V(cat)_3]^{2-}$, $[VO(dmit)_2]^{2-}$, $[V(dmit)_3]^{2-}$; cat = catecholate, dmit = 1,3-dithiole-2-thione-4,5-dithiolate), focusing on the spin–phonon coupling values for the lowest-lying vibrational frequencies and the rigidity of the complex.[115] Spin–phonon couplings are weaker in the vanadyl complexes. Of the four molecules, $[V(cat)_3]^{2-}$ presented the slowest experimental relaxation time, despite the spin–phonon being higher, due to it having the greatest rigidity.

Chilton et al. applied a similar procedure to determine the spin–phonon coupling and vibrational modes involved in spin relaxation, but focusing on mononuclear lanthanide complexes,[79,117-120] especially dysprosocenium derivatives.[101,121] This dysprosocenium family, as mentioned above, comprise the SMMs with the highest blocking temperature. In the case of $[(\eta^5\text{-}Cp^{tBu3})Dy(\eta^5\text{-}Cp^{tBu3})][B(C_6F_5)_4]$, with blocking temperature of 60 K (open hysteresis criterion), the spin–phonon coupling analysis reveals that modes of around 400 cm^{-1} to 500 cm^{-1}, involving the out-of-plane shift of the hydrogen atoms of the cyclopentadienyl ring in non-substituted positions are efficient for spin relaxation.[101] This justifies the completely substituted $[(\eta^5\text{-}Cp^{*})Dy(\eta^5\text{-}Cp^{iPr5})][B(C_6F_5)_4]$ system having a higher blocking temperature (80 K).[103] However, other structural factors are also important, such as the Cp···Dy···Dy angle, because the fully substituted $[(\eta^5\text{-}Cp^{iPr5})Dy(\eta^5\text{-}Cp^{iPr5})][B(C_6F_5)_4]$ complex has a blocking temperature of 66 K.[102]

These methods tend to be computationally demanding since they require several CASSCF calculations along every normal mode. Lower cost approaches to determining spin–phonon coupling constants have been recently proposed.[122,123] In these approaches, only one CASSCF

calculation is required to determine energies and wave functions of the central point, whose crystal-field parameters are extracted using the SIMPRE code,[124] based on effective charge electrostatic calculations. Spin–phonon coupling parameters are determined using the evolution of the Stevens parameters along the distortion induced by each vibrational mode, using the effective charge electrostatic calculations. The comparison shows a reasonable agreement of the spin–phonon constants between this simplified approach[122] and those obtained through CASSCF calculations of the distorted geometries for each vibrational mode.[103] Basically, the new approach allows to identify the key vibrational modes involved in spin relaxation, even though the spin–phonon constants are at energies that differ slightly from the full method.

5. Concluding Remarks

To conclude, it is clear that fundamental theoretical challenges in the study of spin relaxation in molecular systems still remain unsolved. Current efforts point to several directions as: (i) direct and accurate calculation of the relaxation times T_1 and T_2 for molecular qubits; (ii) calculations of the blocking temperature for single-molecule magnets, and development of models that would allow the rationalization of magnitudes that are not correlated with the spin-inversion energy barrier; (iii) a better description of the Raman process with, a clear description of the states involved on such a relaxation process. Furthermore, our understanding of spin–photon coupling will be fundamental to the rationalization of processes in qubits, based on microwave resonators using molecular qubits.

ACKNOWLEDGEMENTS

The research reported herein was supported by the Spanish *Ministerio de Ciencia, Innovación y Universidades* (grants PGC2018-093863-B-C21 and MDM-2017-0767). E.R. thanks the *Generalitat de Catalunya* regional authorities for the grant SGR2017-1289. D.A. thanks the FONDECYT Regular 1170524 project for financial support.

REFERENCES

1. D. Gatteschi, R. Sessoli and J. Villain, Molecular Nanomagnets, Oxford University Press, Oxford, 2006.
2. R. Winpenny (ed.), Molecular cluster magnets, World Scientific Pub. Co, 2012.
3. D. Gatteschi and C. Benelli, Introduction to molecular magnetism : from transition metals to lanthanides, Wiley-VCH, Weinheim, 2015.
4. S. Juan Bartolome, F. Luis, J. F. Fernandez (eds.), Molecular Magnets Physics and Applications, Springer-Verlag Gmb, 2016.
5. B. Sieklucka and D. Pinkowicz (eds.), Molecular magnetic materials : concepts and applications, Wiley-VCH, 2017.
6. M. Holynska (ed.), Single-molecule magnets : molecular architectures and building blocks for spintronics, Wiley, 2019.
7. M. Atzori and R. Sessoli, *J. Am. Chem Soc.*, 2019, **141**, 11339-11352.
8. E. Coronado, *Nat. Rev. Mater.*, 2020, **5**, 87-104.
9. M. Shiddiq, D. Komijani, Y. Duan, A. Gaita-Arino, E. Coronado and S. Hill, *Nature*, 2016, **531**, 348-351.
10. K. S. Pedersen, A. M. Ariciu, S. McAdams, H. Weihe, J. Bendix, F. Tuna and S. Piligkos, *J. Am. Chem Soc.*, 2016, **138**, 5801-5804.
11. M. Atzori, E. Morra, L. Tesi, A. Albino, M. Chiesa, L. Sorace and R. Sessoli, *J. Am. Chem Soc.*, 2016, **138**, 11234-11244.
12. J. M. Zadrozny, J. Niklas, O. G. Poluektov and D. E. Freedman, *ACS Cent. Sci.* 2015, **1**, 488-492.
13. A.-M. Ariciu, D. H. Woen, D. N. Huh, L. E. Nodaraki, A. K. Kostopoulos, C. A. P. Goodwin, N. F. Chilton, E. J. L. McInnes, R. E. P. Winpenny, W. J. Evans and F. Tuna, *Nat. Commun.*, 2019, **10**, 3330.
14. A. Schweiger and G. Jeschke, Principles of pulse electron paramagnetic resonance, Oxford University Press, 2001.
15. S. K. Misra (ed.), Multifrequency electron paramagnetic resonance : theory and applications, Wiley-VCH, 2011.
16. S. K. Misra (ed.), Multifrequency electron paramagnetic resonance : data and techniques, Wiley-VCH, 2014.
17. A. Abragam and B. Bleaney, Electron paramagnetic resonance of transition ions, Oxford Classic Texts in the Physical Sciences, 2013.
18. D. Goldfarb, S. Stoll (eds.), EPR spectroscopy : fundamentals and methods, J. Wiley & Sons, Chicheter, 2018.
19. E. L. Hahn, *Phys. Rev.*, 1950, **80**, 580-594.
20. G. R. Eaton and S. S. Eaton, in *Multifrequency electron paramagnetic resonance : theory and applications*, ed. S. K. Misra, Wiley-VCH, Weinheim, 2011, ch. 17, pp. 719-754.
21. D. Reta and N. F. Chilton, *Phys Chem Chem Phys*, 2019, **21**, 23567-23575.
22. L. T. A. Ho and L. F. Chibotaru, *Phys. Rev. B*, 2016, **94**, 104422.
23. L. T. A. Ho and L. F. Chibotaru, *Phys. Rev. B*, 2018, **98**, 174418.
24. S. Sproules, in *Electron Paramagnetic Resonance, Vol 25*, eds. V. Chechik and D. M. Murphy, 2017, vol. 25, pp. 61-97.
25. M. Atzori, L. Tesi, S. Benci, A. Lunghi, R. Righini, A. Taschin, R. Torre, L. Sorace and R. Sessoli, *J. Am. Chem Soc.*, 2017, **139**, 4338-4341.
26. M. Atzori, L. Tesi, E. Morra, M. Chiesa, L. Sorace and R. Sessoli, *J. Am. Chem Soc.*, 2016, **138**, 2154-2157.

27. C. Bonizzoni, A. Ghirri, M. Atzori, L. Sorace, R. Sessoli and M. Affronte, *Sci. Rep.*, 2017, **7**, 13096.
28. I. Cimatti, L. Bondi, G. Serrano, L. Malavolti, B. Cortigiani, E. Velez-Fort, D. Betto, A. Ouerghi, N. B. Brookes, S. Loth, M. Mannini, F. Totti and R. Sessoli, *Nanoscale Horiz.*, 2019, **4**, 1202-1210.
29. L. Malavolti, M. Briganti, M. Haenze, G. Serrano, I. Cirnatti, G. McMurtrie, E. Otero, P. Ohresser, F. Totti, M. Mannini, R. Sessoli and S. Loth, *Nano. Lett.*, 2018, **18**, 7955-7961.
30. L. Tesi, E. Lucaccini, I. Cimatti, M. Perfetti, M. Mannini, M. Atzori, E. Morra, M. Chiesa, A. Caneschi, L. Sorace and R. Sessoli, *Chem. Sci.*, 2016, **7**, 2074-2083.
31. L. Tesi, A. Lunghi, M. Atzori, E. Lucaccini, L. Sorace, F. Totti and R. Sessoli, *Dalton Trans.*., 2016, **45**, 16635-16643.
32. S. Lenz, H. Bamberger, P. P. Hallmen, Y. Thiebes, S. Otto, K. Heinze and J. van Slageren, *Phys Chem Chem Phys*, 2019, **21**, 6976-6983.
33. S. Bertaina, S. Gambarelli, A. Tkachuk, I. N. Kurkin, B. Malkin, A. Stepanov and B. Barbara, *Nat. Nanotech.*, 2007, **2**, 39-42.
34. Y.-S. Ding, Y.-F. Deng and Y.-Z. Zheng, *Magnetochemistry*, 2016, **2**, 40.
35. J. M. Zadrozny and D. E. Freedman, *Inorg. Chem.*, 2015, **54**, 12027-12031.
36. C. J. Yu, M. J. Graham, J. M. Zadrozny, J. Niklas, M. D. Krzyaniak, M. R. Wasielewski, O. G. Poluektov and D. E. Freedman, *J. Am. Chem Soc.*, 2016, **138**, 14678-14685.
37. M. S. Fataftah, M. D. Krzyaniak, B. Vlaisavljevich, M. R. Wasielewski, J. M. Zadrozny and D. E. Freedman, *Chem. Sci.*, 2019, **10**, 6707-6714.
38. K. Bader, M. Winkler and J. van Slageren, *Chem. Commun.*, 2016, **52**, 3623-3626.
39. S. Lenz, K. Bader, H. Bamberger and J. van Slageren, *Chem. Commun.*, 2017, **53**, 4477-4480.
40. S. Lenz, B. Kern, M. Schneider and J. van Slageren, *Chem. Commun.*, 2019, **55**, 7163-7166.
41. M. Atzori, S. Benci, E. Morra, L. Tesi, M. Chiesa, R. Torre, L. Sorace and R. Sessoli, *Inorg. Chem.*, 2018, **57**, 731-740.
42. A. Ardavan, O. Rival, J. J. L. Morton, S. J. Blundell, A. M. Tyryshkin, G. A. Timco and R. E. P. Winpenny, *Phys. Rev. Lett.*, 2007, **98**, 057201.
43. A. Fernandez, E. M. Pineda, C. A. Muryn, S. Sproules, F. Moro, G. A. Timco, E. J. L. McInnes and R. E. P. Winpenny, *Angew. Chem. Int. Ed.*, 2015, **54**, 10858-10861.
44. J. Ferrando-Soria, E. M. Pineda, A. Chiesa, A. Fernandez, S. A. Magee, S. Carretta, P. Santini, I. J. Vitorica-Yrezabal, F. Tuna, G. A. Timco, E. J. L. McInnes and R. E. P. Winpenny, *Nat. Commun.*, 2016, **7**, 11377.
45. J. Liu, J. Mrozek, W. K. Myers, G. A. Timco, R. E. P. Winpenny, B. Kintzel, W. Plass and A. Ardavan, *Phys. Rev. Lett.*, 2019, **122**, 037202.
46. C. J. Wedge, G. A. Timco, E. T. Spielberg, R. E. George, F. Tuna, S. Rigby, E. J. L. McInnes, R. E. P. Winpenny, S. J. Blundell and A. Ardavan, *Phys. Rev. Lett.*, 2012, **108**, 107204.
47. R. E. P. Winpenny, *Angew. Chem. Int. Ed.*, 2008, **47**, 7992-7994.
48. D. Kaminski, A. L. Webber, C. J. Wedge, J. Liu, G. A. Timco, I. J. Vitorica-Yrezabal, E. J. L. McInnes, R. E. P. Winpenny and A. Ardavan, *Phys. Rev. B*, 2014, **90**, 184419.
49. J. J. Baldovi, S. Cardona-Serra, J. M. Clemente-Juan, E. Coronado, A. Gaita-Arino and H. Prima-Garcia, *Chem. Commun.*, 2013, **49**, 8922-8924.
50. J. J. Baldovi, L. E. Rosaleny, V. Ramachandran, J. Christian, N. S. Dalal, J. M. Clemente-Juan, P. Yang, U. Kortz, A. Gaita-Arino and E. Coronado, *Inorg. Chem. Front.*, 2015, **2**, 893-897.
51. A. Gaita-Arino, F. Luis, S. Hill and E. Coronado, *Nat. Chem.*, 2019, **11**, 301-309.
52. M. D. Jenkins, Y. Duan, B. Diosdado, J. J. Garcia-Ripoll, A. Gaita-Arino, C. Gimenez-Saiz, P. J. Alonso, E. Coronado and F. Luis, *Phys. Rev. B*, 2017, **95**, 064423.
53. J. Lehmann, A. Gaita-Arino, E. Coronado and D. Loss, *Nat. Nanotechn.*, 2007, **2**, 312-317.

54. M. Mariani, F. Borsa, M. J. Graf, S. Sanna, M. Filibian, T. Orlando, K. P. V. Sabareesh, S. Cardona-Serra, E. Coronado and A. Lascialfari, *Phys. Rev. B*, 2018, **97**, 144414.
55. M. J. Martinez-Perez, S. Cardona-Serra, C. Schlegel, F. Moro, P. J. Alonso, H. Prima-Garcia, J. M. Clemente-Juan, M. Evangelisti, A. Gaita-Arino, J. Sese, J. van Slageren, E. Coronado and F. Luis, *Phys. Rev. Lett.*, 2012, **108**, 247213.
56. R. Hussain, G. Allodi, A. Chiesa, E. Garlatti, D. Mitcov, A. Konstantatos, K. S. Pedersen, R. De Renzi, S. Piligkos and S. Carretta, *J. Am. Chem Soc.*, 2018, **140**, 9814-9818.
57. M. D. Jenkins, D. Zueco, O. Roubeau, G. Aromí, J. Majer and F. Luis, *Dalton Trans.*, 2016, **45**, 16682-16693.
58. C. Bonizzoni, A. Ghirri, K. Bader, J. van Slageren, M. Perfetti, L. Sorace, Y. Lan, O. Fuhr, M. Ruben and M. Affronte, *Dalton Trans.*, 2016, **45**, 16596-16603.
59. M. V. G. Dutt, L. Childress, L. Jiang, E. Togan, J. Maze, F. Jelezko, A. S. Zibrov, P. R. Hemmer and M. D. Lukin, *Science*, 2007, **316**, 1312-1316.
60. A. Jarmola, V. M. Acosta, K. Jensen, S. Chemerisov and D. Budker, *Phys. Rev. Lett.*, 2012, **108**, 197601.
61. E. D. Herbschleb, H. Kato, Y. Maruyama, T. Danjo, T. Makino, S. Yamasaki, I. Ohki, K. Hayashi, H. Morishita, M. Fujiwara and N. Mizuochi, *Nat. Commun.*, 2019, **10**, 3766.
62. J. H. Van Vleck, *Phys. Rev.*, 1940, **57**, 426-447.
63. S. Gómez-Coca, A. Urtizberea, E. Cremades, P. J. Alonso, A. Camón, E. Ruiz and F. Luis, *Nat. Commun.*, 2014, **5**, 4300.
64. K. J. Standley and R. A. Vaughan, Electron spin relaxation phenomena in solids, Hilger, London, 1969.
65. J. W. Orton, J. W. Orton and J. W. Orton, Electron paramagnetic resonance : an introduction to transition group ions in crystals, Gordon and Breach, New York, N.Y, 1969.
66. P. L. Scott and C. D. Jeffries, *Phys. Rev.*, 1962, **127**, 32-51.
67. L. T. A. Ho and L. F. Chibotaru, *Phys. Rev. B*, 2018, **97**, 024427.
68. A. Chiesa, F. Cugini, R. Hussain, E. Macaluso, G. Allodi, E. Garlatti, M. Giansiracusa, C. A. P. Goodwin, F. Ortu, D. Reta, J. M. Skelton, T. Guidi, P. Santini, M. Solzi, R. De Renzi, D. P. Mills, N. F. Chilton and S. Carretta, *Phys.Rev. B*, 2020, **101**, 174402.
69. S. S. Eaton, J. Harbridge, G. A. Rinard, G. R. Eaton and R. T. Weber, *Appl Magn Reson*, 2001, **20**, 151-157.
70. N. Bloembergen, E. M. Purcell and R. V. Pound, *Phys. Rev.*, 1948, **73**, 679-712.
71. K. K. P. Srivastava and H. C. Singh, *Phys. Status Solidi B,*, 1980, **101**, 43-49.
72. J. Ruiz, A. J. Mota, A. Rodriguez-Dieguez, S. Titos, J. M. Herrera, E. Ruiz, E. Cremades, J. P. Costes and E. Colacio, *Chem Commun*, 2012, **48**, 7916-7918.
73. Y. Kishi, F. Pointillart, B. Lefeuvre, F. Riobé, B. Le Guennic, S. Golhen, O. Cador, O. Maury, H. Fujiwara and L. Ouahab, *Chem Commun*, 2017, **53**, 3575-3578.
74. F. Pointillart, K. Bernot, S. Golhen, B. Le Guennic, T. Guizouarn, L. Ouahab and O. Cador, *Angew Chem Int Ed*, 2015, **54**, 1504-1507.
75. D. Aravena, *J. Phys. Chem. Lett.*, 2018, **9**, 5327-5333.
76. N. V. Prokof'ev and P. C. E. Stamp, *Phys. Rev. Lett.*, 1998, **80**, 5794-5797.
77. W. Wernsdorfer, T. Ohm, C. Sangregorio, R. Sessoli, D. Mailly and C. Paulsen, *Phys. Rev. Lett.*, 1999, **82**, 3903-3906.
78. R. J. Blagg, L. Ungur, F. Tuna, J. Speak, P. Comar, D. Collison, W. Wernsdorfer, E. J. L. McInnes, L. F. Chibotaru and R. E. P. Winpenny, *Nat. Chem.*, 2013, **5**, 673-678.
79. Y. S. Ding, K. X. Yu, D. Reta, F. Ortu, R. E. P. Winpenny, Y. Z. Zheng and N. F. Chilton, *Nat. Commun.* 2018, **9**, 3134.
80. O. Eriksson, A. Bergman, L. Bergqvist and J. Hellsvik, Atomistic spin dynamics : foundations and applications, Oxford University Press, Oxford, United Kingdom, 2017.
81. H. Hammar and J. Fransson, *Phys. Rev. B*, 2017, **96**, 214401.
82. L. Escalera-Moreno, A. Gaita-Arino and E. Coronado, *Phys. Rev. B*, 2019, **100**, 064405.
83. P. C. E. Stamp and I. S. Tupitsyn, *Phys. Rev. B,*, 2004, **69**, 014401.
84. L. Escalera-Moreno and J. J. Baldovi, *Front. Chem.*, 2019, **7**, 662.

85. J. Chen, C. Hu, J. F. Stanton, S. Hill, H.-P. Cheng and X.-G. Zhang, *J. Phys. Chem. Lett.*, 2020, **11**, 2074-2078.
86. M. J. Graham, M. D. Krzyaniak, M. R. Wasielewski and D. E. Freedman, *Inorg. Chem.*, 2017, **56**, 8106-8113.
87. M. J. Graham, C.-J. Yu, M. D. Krzyaniak, M. R. Wasielewski and D. E. Freedman, *J. Am. Chem Soc.*, 2017, **139**, 3196-3201.
88. W. Yang and R.-B. Liu, *Phys. Rev. B*, 2008, **78**, 085315.
89. P. P. Hallmen, H.-J. Werner, D. Kats, S. Lenz, G. Rauhut, H. Stoll and J. van Slageren, *Phys. Chem. Chem. Phys.*, 2019, **21**, 9769-9778.
90. E. Moreno Pineda, N. F. Chilton, R. Marx, M. Dörfel, D. O. Sells, P. Neugebauer, S.-D. Jiang, D. Collison, J. van Slageren, E. J. L. McInnes and R. E. P. Winpenny, *Nat. Commun.*, 2014, **5**, 5243.
91. M. J. Giansiracusa, E. Moreno-Pineda, R. Hussain, R. Marx, M. Martínez Prada, P. Neugebauer, S. Al-Badran, D. Collison, F. Tuna, J. van Slageren, S. Carretta, T. Guidi, E. J. L. McInnes, R. E. P. Winpenny and N. F. Chilton, *J. Am. Chem. Soc.* 2018, **140**, 2504-2513.
92. M. E. Lines, *J. Chem. Phys.*, 1971, **55**, 2977-2984.
93. L. F. Chibotaru, L. Ungur and A. Soncini, *Angew. Chem. Int. Ed.*,, 2008, **47**, 4126-4129.
94. L. F. Chibotaru, in *Molecular Nanomagnets and Related Phenomena*, ed. S. Gao, 2015, vol. 164, pp. 185-229.
95. L. F. Chibotaru and L. Ungur, *J Chem Phys*, 2012, **137**, 064112.
96. I. F. Galvan, M. Vacher, A. Alavi, C. Angeli, F. Aquilante, J. Autschbach, J. J. Bao, S. I. Bokarev, N. A. Bogdanov, R. K. Carlson, L. F. Chibotaru, J. Creutzberg, N. Dattani, M. G. Delcey, S. J. S. Dong, A. Dreuw, L. Freitag, L. M. Frutos, L. Gagliardi, F. Gendron, A. Giussani, L. Gonzalez, G. Grell, M. Y. Guo, C. E. Hoyer, M. Johansson, S. Keller, S. Knecht, G. Kovacevic, E. Kallman, G. Li Manni, M. Lundberg, Y. J. Ma, S. Mai, J. P. Malhado, P. A. Malmqvist, P. Marquetand, S. A. Mewes, J. Norell, M. Olivucci, M. Oppel, Q. M. Phung, K. Pierloot, F. Plasser, M. Reiher, A. M. Sand, I. Schapiro, P. Sharma, C. J. Stein, L. K. Sorensen, D. G. Truhlar, M. Ugandi, L. Ungur, A. Valentini, S. Vancoillie, V. Veryazov, O. Weser, T. A. Wesolowski, P. O. Widmark, S. Wouters, A. Zech, J. P. Zobel and R. Lindh, *J. Chem. Theor. Comput.*, 2019, **15**, 5925-5964.
97. L. Ungur and L. F. Chibotaru, *Chem. Eur. J.*, 2017, **23**, 3708-3718.
98. V. Vieru, L. Ungur and L. F. Chibotaru, *J. Phys. Chem. Lett.*, 2013, **4**, 3565-3569.
99. N. F. Chilton, C. A. P. Goodwin, D. P. Mills and R. E. P. Winpenny, *Chem. Commun.*, 2015, **51**, 101-103.
100. S. Gomez-Coca, D. Aravena, R. Morales and E. Ruiz, *Coord. Chem. Rev.*, 2015, **289**, 379-392.
101. C. A. P. Goodwin, F. Ortu, D. Reta, N. F. Chilton and D. P. Mills, *Nature*, 2017, **548**, 439-442.
102. K. Randall McClain, C. A. Gould, K. Chakarawet, S. J. Teat, T. J. Groshens, J. R. Long and B. G. Harvey, *Chem. Sci.*, 2018, **9**, 8492-8503.
103. F. S. Guo, B. M. Day, Y. C. Chen, M. L. Tong, A. Mansikkamaki and R. A. Layfield, *Science*, 2018, **362**, 1400-1403.
104. Y.-S. Ding, N. F. Chilton, R. E. P. Winpenny and Y.-Z. Zheng, *Angew. Chem. Int. Ed.*, 2016, **55**, 16071-16074.
105. L. Llanos and D. Aravena, *J. Magn. Magn. Mater.*, 2019, **489**, 165456.
106. A. Castro-Alvarez, Y. Gil, L. Llanos and D. Aravena, *Inorg. Chem. Front.*, 2020, doi:10.1039/D0QI00487A.
107. S. Demir, I.-R. Jeon, J. R. Long and T. D. Harris, *Coord. Chem. Rev.*, 2015, **289-290**, 149-176.
108. A. Lunghi and S. Sanvito, *Sci. Adv.*, 2019, **5**, eaax7163.
109. L. Escalera-Moreno, J. J. Baldov, A. Gaita-Arino and E. Coronado, *Chem. Sci.*, 2018, **9**, 3265-3275.

110. L. Escalera-Moreno, N. Suaud, A. Gaita-Arino and E. Coronado, *J. Phys. Chem. Lett.*, 2017, **8**, 1695-1700.
111. L. Escalera-Moreno, J. J. Baldovi, A. Gaita-Arino and E. Coronado, *Inorg. Chem.*, 2019, **58**, 11883-11892.
112. R. Mirzoyan and R. G. Hadt, *Phys. Chem. Chem. Phys.*, 2020, doi:10.1039/D0CP00852D..
113. A. Lunghi, F. Totti, S. Sanvito and R. Sessoli, *Chem. Sci.*, 2017, **8**, 6051-6059.
114. A. Lunghi, F. Totti, R. Sessoli and S. Sanvito, *Nat. Commun.*, 2017, **8**, 14620.
115. A. Albino, S. Benci, L. Tesi, M. Atzori, R. Torre, S. Sanvito, R. Sessoli and A. Lunghi, *Inorg. Chem.*, 2019, **58**, 10260-10268.
116. A. Lunghi and S. Sanvito, *J. Magn. Magn. Mater.*, 2019, **487**, Unsp 165325.
117. P. Evans, D. Reta, G. F. S. Whitehead, N. F. Chilton and D. P. Mills, *J. Am. Chem Soc.*, 2019, **141**, 19935-19940.
118. C. A. P. Goodwin, D. Reta, F. Ortu, J. J. Liu, N. F. Chilton and D. P. Mills, *Chem. Commun.*, 2018, **54**, 9182-9185.
119. J. J. Liu, D. Reta, J. A. Cleghorn, Y. X. Yeoh, F. Ortu, C. A. P. Goodwin, N. F. Chilton and D. P. Mills, *Chem. Eur. J.*, 2019, **25**, 7749-7758.
120. F. Ortu, D. Reta, Y. S. Ding, C. A. P. Goodwin, M. P. Gregson, E. J. L. McInnes, R. E. P. Winpenny, Y. Z. Zheng, S. T. Liddle, D. P. Mills and N. F. Chilton, *Dalton Trans.*, 2019, **48**, 8541-8545.
121. C. A. P. Goodwin, D. Reta, F. Ortu, N. F. Chilton and D. P. Mills, *J. Am. Chem Soc.*, 2017, **139**, 18714-18724.
122. A. Ullah, J. Cerda, J. J. Baldovi, S. A. Varganov, J. Arago and A. Gaita-Arino, *J. Phys. Chem. Lett.*, 2019, **10**, 7678-7683.
123. L. Escalera-Moreno, J. J. Baldovi, A. Gaita-Arino and E. Coronado, *Chem. Sci.*, 2020, **11**, 1593-1598.
124. S. Cardona-Serra, L. Escalera-Moreno, J. J. Baldovi, A. Gaita-Arino, J. M. Clemente-Juan and E. Coronado, *J. Comput. Chem.*, 2016, **37**, 1238-1244.